The location of large-scale soil moisture anomalies affects moisture transport and precipitation over southeastern South America

Chu-Chun Chen[1] **and Francina Dominguez**[1]

[1]Department of Atmospheric Sciences, University of Illinois Urbana–Champaign, Urbana, IL 61801

Key Points:

- The impact of dry soil moisture anomalies (SMAs) on Southeastern South America (SESA) regional climate is sensitive to the location of SMAs
- This study provides a causal mechanism linking soil moisture to precipitation via atmospheric circulation
- When western SESA has dry soil, it generates anomalous geostrophic wind, which is co-located with the low-level jet exit region

Corresponding author: Francina Dominguez, `francina@illinois.edu`

Abstract

Southeastern South America (SESA) is a highly productive agricultural region and a hot spot for land-atmosphere interactions. To evaluate the impact of dry soil moisture anomalies (SMAs) on SESA climate and the sensitivity of the regional climate response to the location of SMAs, we perform three experimental simulations using the Community Earth System Model (CESM) with prescribed dry SMAs over (1) SESA, (2) western SESA, and (3) eastern SESA. The dry eastern SESA simulation shows widespread negative precipitation anomalies. In contrast, the dry western SESA simulation shows positive precipitation anomalies over northeastern Argentina, which are associated with the enhanced southward moisture flux co-located with the South American low-level jet exit region. A composite analysis of extremely dry cases over western SESA using reanalysis data agrees with the findings from our CESM experiment. These findings have potential implications for subseasonal forecasting in this region.

Plain Language Summary

Large-scale soil moisture anomalies evolve slowly and can provide an opportunity for better forecasting at time scales longer than two weeks. Therefore, it is critical to understand the causal physical mechanism and evaluate whether the regional climate response is sensitive to the location of soil moisture anomalies, especially in a productive agricultural region like southeastern South America (SESA). Using a numerical climate model, we simulate the impacts of dry soil over (1) SESA, (2) western SESA, and (3) eastern SESA. The simulations show that dry soil over Western SESA can alter regional atmospheric circulation in the proximity of the existing corridor of poleward moisture transport, hence enhancing rainfall over northeastern Argentina. Conversely, dry soil over eastern SESA or the entire SESA region results in less precipitation because enhanced northerly transport is not co-located with the low-level wind corridor. Analysis of a dataset that incorporates observations supports our findings from numerical simulations.

1 Introduction

Southeastern South America (SESA) is one of the most productive agricultural regions on Earth (FAO, 2016). The region is also critical for hydroelectric power and has large population centers (Barros et al., 2006). Herein, improved precipitation predictability in SESA could have far-reaching socioeconomic impacts. Land-atmosphere interactions are a promising avenue for improved predictability (Koster et al., 2011; Guo et al., 2011; Dirmeyer et al., 2018), as soil moisture anomalies (SMAs) evolve on the subseasonal to seasonal time scales. As such, understanding how SMAs affect precipitation can potentially narrow the weather-climate prediction gap (Mariotti et al., 2018). SESA has been recognized as a hot spot for land-atmosphere interactions in satellite products, reanalysis data, and climate models (e.g., Ruscica et al., 2016; Spennemann et al., 2018; Baker et al., 2021). Through land-atmosphere interactions, large-scale SMAs can alter regional climate (e.g., Shukla & Mintz, 1982; Koster et al., 2014; Teng et al., 2019); one of the pathways is by changing the atmospheric circulation and associated moisture transport (Oglesby & Erickson, 1989; Grimm et al., 2007; Yang & Dominguez, 2019; Bieri et al., 2021). An important moisture source for SESA is the moisture transported from lower latitudes, which is closely related to South American low-level jet (SALLJ) activity (Nicolini et al., 2002; Marengo et al., 2004; Vera et al., 2006; Salio et al., 2007; Arraut et al., 2012). Previous studies have shown that intense rainfall events in SESA are linked to low-level jet activity (Monaghan et al., 2010).

The effect of the land surface on South America's overlying atmosphere has been quantified using different coupling metrics (Spennemann & Saulo, 2015; Sörensson & Menéndez, 2011; Ruscica et al., 2015). These metrics highlight regions of positive soil moisture-precipitation feedbacks over the South Atlantic Convergence Zone (Spennemann & Saulo, 2015) and eastern SESA (Sörensson & Menéndez, 2011), and negative feedbacks over western SESA (Sörensson & Menéndez, 2011). The location-dependent results from these studies imply that the precipitation response to SMAs is sensitive to the location of SMAs. However, because these coupling metrics are calculated grid point by grid point, neither the location where large-scale SMAs strongly influence regional climate nor the underlying mechanisms can be identified.

Previous studies have proposed mechanisms to explain how dry SMAs can affect moisture transport and precipitation. Global climate model experiments show that dry SMAs over SESA lead to anomalous cyclonic circulation and enhanced moisture transport and precipitation over SESA at monthly time scales (Bieri et al., 2021). At daily time scales, regional model simulations were used to investigate the effect of dry SMAs over northwestern Argentina (Saulo et al., 2010; Yang & Dominguez, 2019). While Yang and Dominguez (2019) have found corresponding enhanced northerly moisture transport and consequently increased precipitation, Saulo et al. (2010) did not find consistent wind anomalies in the dry northwest Argentina experiment, which may be attributed to the shorter simulation period. An analogous study, using observations of remotely sensed vegetation indices, demonstrates that increased precipitation over SESA can be linked to intensified northerly moisture flux, which is the geostrophic response to the pressure gradient induced by negative vegetation index anomalies over northern Argentina (Chug & Dominguez, 2019). Similar mechanisms have also been identified in other parts of the world, including the Great Plains of the United States (Campbell et al., 2019; Matus et al., 2023) and Africa (Talib et al., 2022, 2023).

However, comparison among these previous studies is challenging because of (1) the diversity in the numerical models employed and the approaches taken and (2) the lack of consistent sensitivity tests for different locations of soil moisture forcing, such as the experiments done for North America (Koster et al., 2016; Teng et al., 2019). Therefore, in this study, we performed idealized experiments using the Community Earth System Model version 1 (CESM1) (Hurrell et al., 2013) that prescribe dry SMAs within SESA, western SESA, and eastern SESA to assess the sensitivity of moisture transport and precipitation response to SMAs at different locations. In addition to the idealized experiments, we also analyze the extremely dry cases using the European Centre for Medium-Range Weather Forecast (ECMWF) Reanalysis v5 (ERA5) (Hersbach et al., 2020) monthly dataset to present observational evidence for our numerical experiments. The goal of this study is to understand the mechanisms by which dry SMAs affect moisture transport and precipitation over SESA and to assess the influence of the location of SMAs.

2 Data and methods

2.1 Model experiments

In this study, we use the CESM1 and follow a similar model setup as in Teng et al. (Teng et al., 2019). CESM1 consists of atmosphere, ocean, land, sea ice, and land ice components. In our simulation setup, the model has 30 vertical levels and a horizontal resolution of approximately 1° (0.9° × 1.25°). Since we focus on the land-atmosphere interactions, we used the "F1850LENS" component set, which activates land and atmosphere components while deactivating or prescribing other components. The sea surface temperatures and sea ice concentrations are prescribed using the monthly mean climatology averaged over years 402-1510 of the fully coupled preindustrial control run of the CESM1 large ensemble project (Kay et al., 2015).

We performed one control simulation and three experimental simulations, each comprising 30 ensemble members initialized with varying initial conditions. The 30 initial conditions are taken from the last 500 years (at least five years apart) of the atmosphere/land-only control run of the CESM1 large ensemble project. For the control simulation, each ensemble member was initialized from January and ended after running for 15 months. For the three experimental simulations, within selected domains, we prescribed the entire column of soil water to zero at each time step. As shown in Fig. 1a, 2a, and S1a, the domains we selected are (1) SESA (67°W-45°W, 24°S-40°S), (2) western SESA (67°W-60°W, 24°S-40°S), and (3) eastern SESA (60°W-45°W, 24°S-40°S). The experimental simulations started from September (using the restart files from control simulations) and ended after running for 7 months, covering austral spring to early fall, because land-atmosphere interactions are stronger during summer (Koster & Suarez, 1995).

2.2 Data

To validate the simulated results, we used monthly ERA5 data spanning the period 1979 to 2021. ERA5 reanalysis assimilates various sources of observations into the Integrated Forecasting System Cy41r2 model, providing a complete global estimate and a wide range of meteorological variables with 37 vertical pressure levels and a horizontal resolution of 0.25 degrees. Root-zone soil moisture is calculated via a weighted average based on the soil layer thickness of the top three layers of volumetric soil water (layer 1: 0-7cm, layer 2: 7-28cm, layer 3: 28-100cm).

2.3 Extremely dry cases selection

We compare our idealized experiments with extremely dry cases from ERA5 reanalysis to verify the simulated results. First, we chose months between October and January because we focus on seasons with relatively strong land-atmosphere interactions. Second, we calculated the SMAs of each month by removing the monthly climatology averaged from 1981 to 2010. Third, we ranked the area-averaged root-zone SMAs over western SESA and selected the driest 3% months during the study period (Table S1). In these extremely dry cases, we then calculated the composite anomalies of surface heat fluxes and other atmospheric variables corresponding to the month following the dry soil moisture months. The significance of the differences between extremely dry cases and climatology was determined using the Student's t-test.

3 Results

3.1 CESM simulations

Fig. 1 shows the difference between the ensemble average of the dry SESA simulations and the control simulations in December; area-averaged values are shown in Table S2. The dry SMAs decrease the surface latent heat flux significantly because of the reduction of available water from the soil (Fig. 1a and b). Since the change in incoming radiation (net shortwave radiation and upwelling longwave radiation) is small (Table S2), the surface temperature and the surface sensible heat flux increase (Fig. 1c) to compensate for the decrease in surface latent heat flux, which consequently increase 2-m temperature (Fig. 1d). Warming near the surface induces a thermal low and lower geopotential heights at 850 hPa within SESA (Figs. 1e and f). In addition, the warming increases the thickness

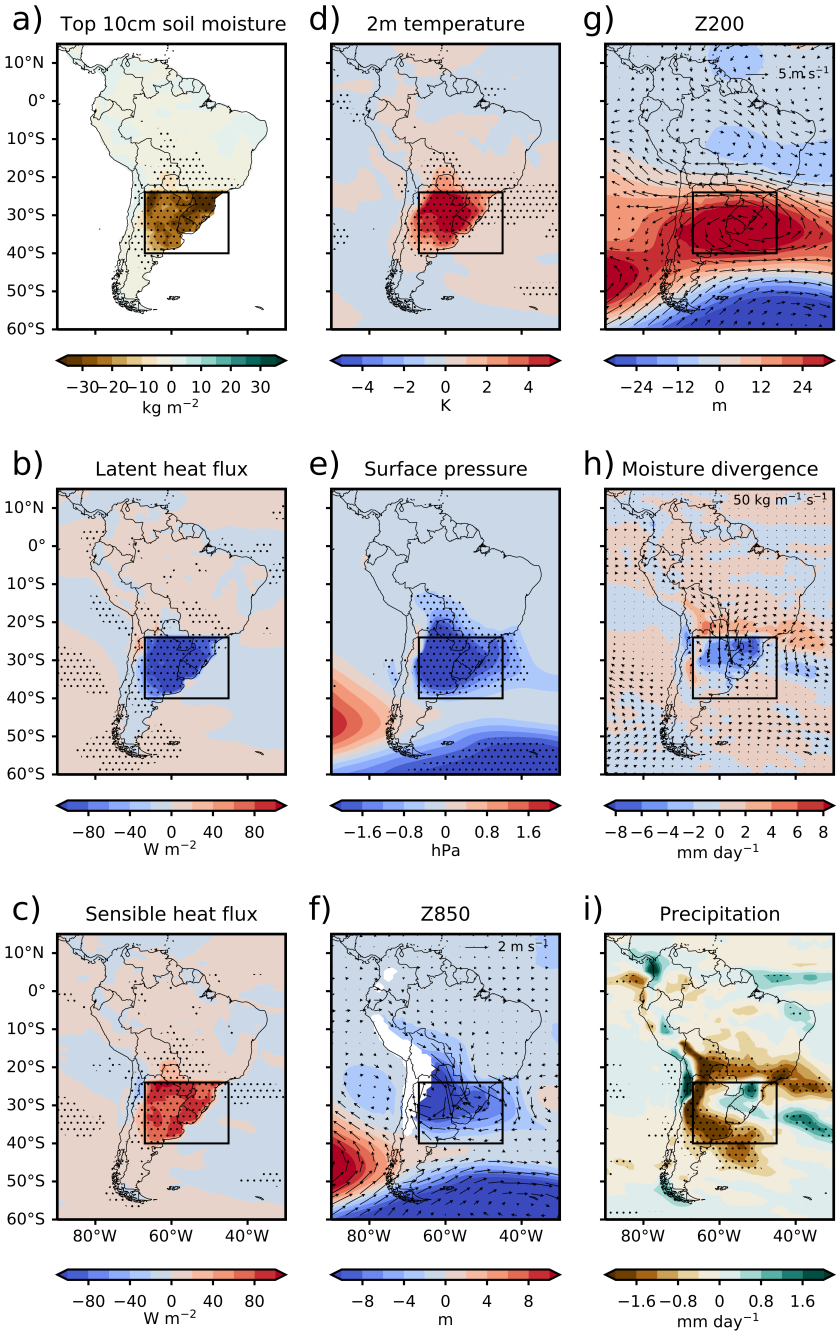

Figure 1. Difference between the ensemble average of the dry SESA simulations and the control simulations in December (a) soil water in top 10 cm, (b) surface latent heat flux, (c) surface sensible heat flux, (d) 2-m temperature, (e) surface pressure, (f) geopotential height and wind at 850 hPa, (g) geopotential height and wind at 200 hPa, (h) vertically integrated moisture flux divergence and moisture flux, and (i) precipitation. The box indicates the region for which the idealized soil moisture anomalies are prescribed. Stippling indicates statistically significant differences (p-value less than or equal to 0.05).

in the lower troposphere, leading to an increase in the geopotential heights at the upper level (Fig. 1g). The difference in vertically integrated moisture flux shows an enhanced southward moisture flux into SESA, and moisture flux converges over northern Argentina and southern Brazil (blue shading in Fig. 1h). The precipitation decreases over central and northwestern Argentina but increases over southern Brazil (Fig. 1i). The increased precipitation corresponds to the strongest moisture flux convergence.

We further investigate if the dry SMAs in the western and eastern parts of SESA have different impacts. Fig. 2 shows the difference between the ensemble average of the dry western SESA simulations and the control simulations in December; area-averaged values are shown in Table S3. Dry SMAs over western SESA also reduce the surface latent heat flux (Fig. 2a and b) and increase the surface sensible heat flux (Fig. 2c) within the domain. The 2-m temperature increases as well (Fig. 2d), but the magnitude is smaller than that in the dry SESA run. The surface pressure and 850 hPa geopotential height decrease mostly within the domain (Figs. 2e and f). On the other hand, geopotential height at 200 hPa increases over the southern part of the domain and neighboring regions, suggesting potential nonlocal effects (Fig. 2g). The southward vertically integrated moisture flux and anomalous moisture flux convergence intensify (Fig. 2h), corresponding to increased precipitation over northeastern Argentina (Fig. 2i). The region with negative precipitation anomalies is narrower compared to the anomalies observed in the dry SESA run (Figs. 2i and 1i).

Fig. S1 shows the difference between the ensemble average of the dry eastern SESA simulations and the control simulations in December; area-averaged values are shown in Table S4. Similar to the responses in the dry SESA run and the dry western SESA run, the surface latent heat flux decreases because of the dry SMAs (Fig. S1a and b), and the surface sensible heat flux and 2-m temperature increase (Figs. S1c and d), although the anomalies extend slightly to the west of the eastern SESA domain. The dry eastern SESA run also has lower surface pressure and lower geopotential height at 850 hPa over the domain and the surrounding regions compared to the control run (Figs. S1e and f). There is a positive geopotential height anomaly at 200 hPa as well, with larger anomalies over the eastern part of the domain (Fig. S1g). Although there is moisture flux convergence within the domain, there is a weaker anomalous southward vertically integrated moisture flux into SESA (Fig. S1h) compared with that in the dry western SESA run (Fig. 2h). The area with negative precipitation anomalies is larger compared with the dry western SESA run, covering the central Andes, northern Argentina, and Paraguay, while only a small portion of southern Brazil shows positive precipitation anomalies (Fig. S1i).

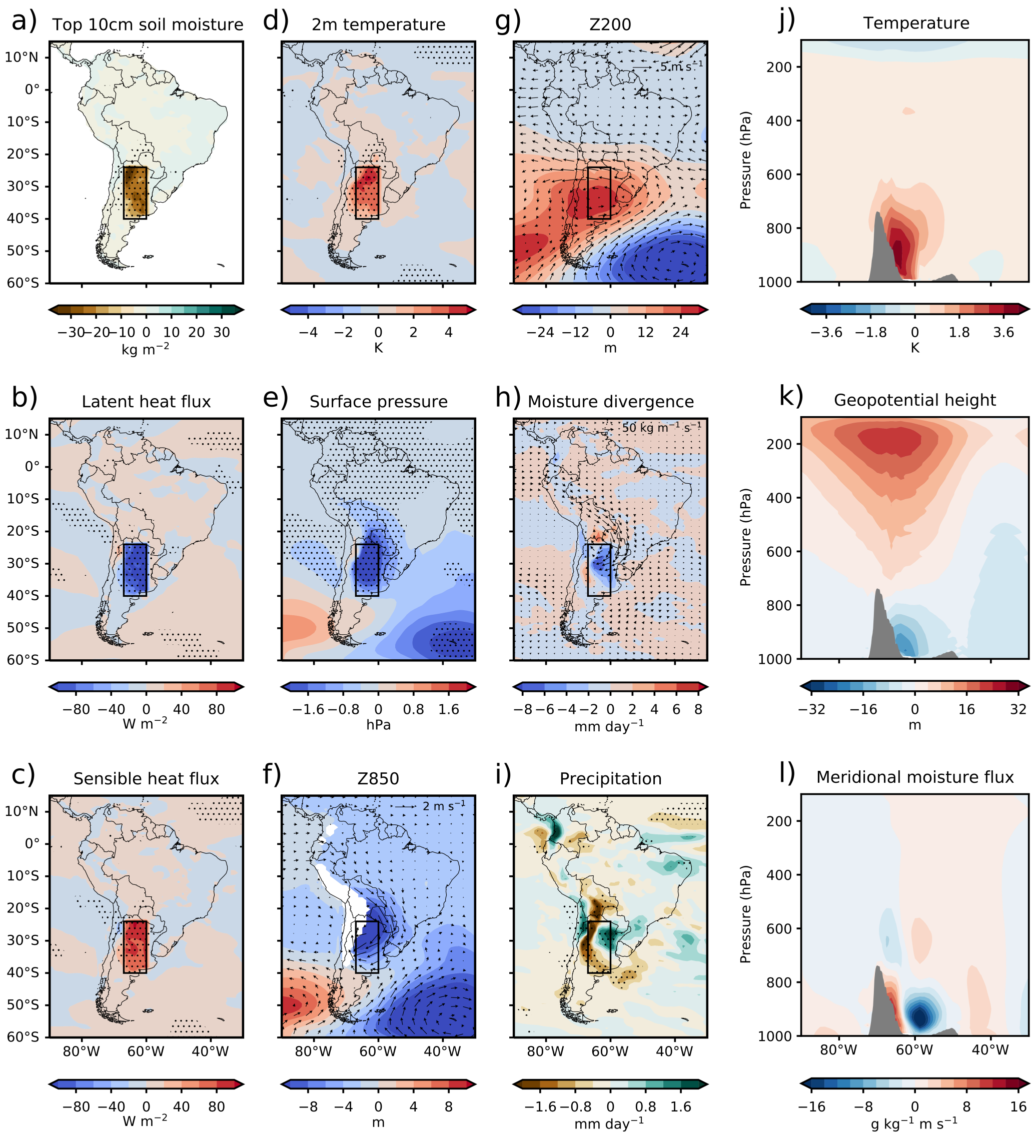

Figure 2. (a) to (i) as in Fig. 1, but for the dry western SESA simulations. Vertical cross sections of (j) temperature, (k) geopotential height, and (l) meridional moisture flux are anomalies between the ensemble average of the dry western SESA simulations and the control simulations in December. Gray shading indicates the topography. Values in vertical cross sections have the same longitude range as in (a) to (i) and are averaged between 24°S and 40°S.

We further examine pressure-longitude cross sections averaged between 24°S and 40°S. Figures 2j-l show the difference in temperature, geopotential height, and meridional moisture flux between the dry western SESA run and the control run in December. Warming at the surface and lower troposphere (Fig. 2j) decreases lower-level and increases upper-level geopotential heights (Fig. 2k) over the western SESA. The baroclinicity and the zonal gradient of the geopotential height influence the meridional moisture transport on both sides of the domain: on the eastern boundary of the domain, the positive zonal gradient of low-level geopotential height anomalies leads to enhanced low-level southward moisture flux; on the western boundary of the domain, the negative zonal gradient of low-level geopotential height anomalies weakens low-level southward moisture flux (Fig. 2l). The control run and the dry western SESA run show that the low-level southward moisture flux accelerates on the eastern boundary of the domain and decelerates on the western boundary of the domain, although the deceleration is inconspicuous because it is close to the mountain regions (Fig. S2). Critically, the enhanced low-level southward moisture flux in the dry western SESA run (Fig. 2l) is co-located with the strong southward moisture flux in the control run (Fig. S2a). Similar responses can be observed in the dry SESA run (Fig. S3) and the dry eastern SESA run (Fig. S4). However, unlike the western SESA case, the enhanced southward moisture flux in the SESA and eastern SESA runs does not correspond to the location of the southward moisture flux over land in the control run (Figs. S3c, S4c, and S2a). Additionally, in the dry eastern SESA run, the western boundary of the domain exhibits an anomalous northward flux (Fig. S4c), which then leads to the widespread negative precipitation anomalies (Fig. S1i). The distinct responses among experimental runs highlight the sensitivity of precipitation and moisture transport to the location of SMAs over SESA.

3.2 ERA5 reanalysis

Fig. 3 shows the difference between the extremely dry cases and climatology; area-averaged values are shown in Table S5. Antecedent SMAs over western SESA (Fig. 3a) are associated with decreased surface latent heat flux (Fig. 3b) and increased surface sensible heat flux (Fig. 3c) within the same domain. The 2-m temperature increases over northern Argentina and neighboring areas (Fig. 3d), which is similar to the response in the dry western SESA CESM1 simulation (Fig. 2d). There are negative surface pressure anomalies and lower geopotential height anomalies at 850 hPa mostly over the western SESA (Figs. 3e and f), while the geopotential height at 200 hPa increases over the entire SESA (Fig. 3g). The anomalous moisture convergence over northeastern Argentina and Paraguay (Fig. 3h) corresponds to increased precipitation over the same region (Fig. 3i).

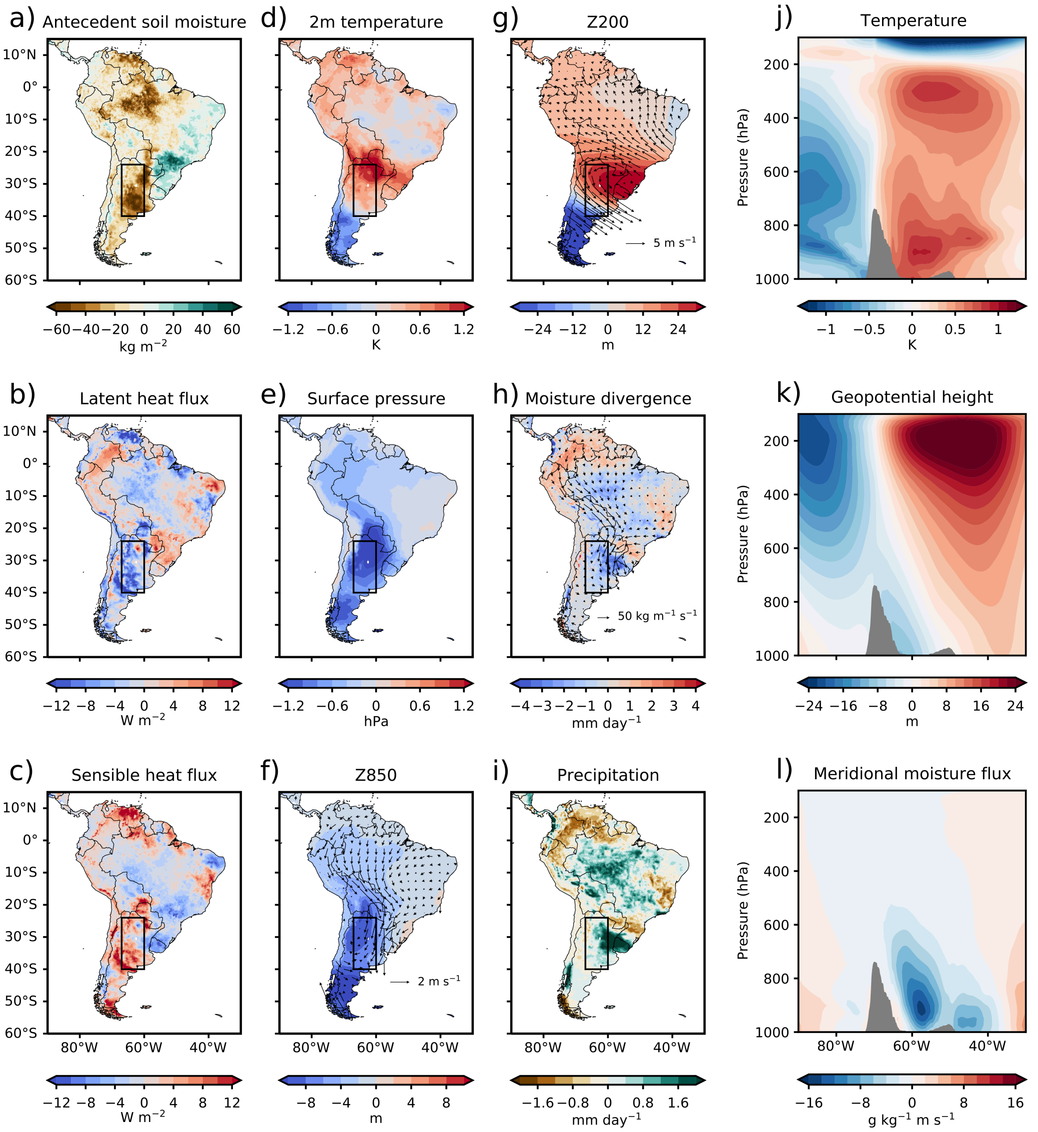

Figure 3. (b) to (l) as in Fig. 2, but for the difference between the ERA5 reanalysis extremely dry western SESA cases and climatology. (a) is the difference in antecedent soil moisture in top 1 m.

Fig. 3j-l shows pressure-longitude cross sections of temperature, geopotential height, and meridional moisture flux anomalies averaged between 24°S and 40°S in the extremely dry western SESA cases compared to climatology. There is warming at both the lower troposphere and the upper troposphere (Fig. 3j), and the low-level warming corresponds to decreased low-level geopotential height over western SESA (Fig. 3k). On the east side of the domain, the positive zonal gradient of low-level geopotential height also corresponds to intensified southward moisture flux, although there is no apparent deceleration on the west side of the domain (Fig. 3l).

Overall, the responses in ERA5 reanalysis and in CESM simulations are quite similar. Slight differences between the extremely dry cases and the idealized experimental runs are reasonable because the responses in the extremely dry cases are a combination of signals from SMAs and other forcings.

4 Discussion

The results from our CESM simulations and ERA5 reanalysis suggest that dry SMAs can lead to lower troposphere warming and geopotential height anomalies, causing anomalous geostrophic flows, which can influence moisture fluxes and precipitation over SESA. This is consistent with previous studies that show that the thermal low induced by dry SMAs affects local circulation and further influences precipitation (Grimm et al., 2007; Chug & Dominguez, 2019; Yang & Dominguez, 2019; Bieri et al., 2021). It is also supported by previous studies that these circulation changes could be linked to the northwestern Argentinean low and the SALLJ (Chug & Dominguez, 2019; Yang & Dominguez, 2019). Note that Chug and Dominguez (2019) focus on observed vegetation index anomalies instead of SMAs, but the browning (negative) vegetation index anomalies are located over western SESA and have similar surface forcings (surface latent heat flux, surface sensible heat flux, and surface temperature) and atmospheric responses (thermal low, southerly wind, and precipitation) as the results shown in the western SESA experiment.

One of the implications of this work is that the relation between soil moisture and precipitation can affect the length and intensity of droughts, which is also discussed in Bieri et al. (2021). In this study, we suggest that this relation is sensitive to the location of dry SMAs, and we clearly identify the physical mechanisms at play. The dry SMAs over the entire SESA or over the eastern SESA mostly induce a positive feedback between soil moisture and precipitation (i.e., dry soil leads to less precipitation, then less precipitation leads to drier soil), which has been the focus of most previous studies (e.g., Shukla & Mintz, 1982; Findell & Eltahir, 1997; Eltahir, 1998; Seneviratne et al., 2010). This positive feedback may result in a longer or stronger drought. On the contrary, the dry SMAs over the western

SESA induce a negative feedback between soil moisture and precipitation over most of the region, indicating that the dry soil is associated with positive precipitation anomalies, which would mitigate the dry SMAs. This negative feedback may lead to a shorter and weaker drought. Note that the precipitation responses are not exactly over the dry SMAs domain, so in addition to the changes in length and intensity, the drought may also migrate with time.

There are some limitations in this study related to the simulation setup. First, our idealized experiments prescribe extremely dry SMAs. Teng et al. (2019) have performed a sensitivity test of different strengths of soil moisture forcing over the Great Plains and found that there are clear and robust upper-level geopotential responses in the extremely dry simulations, while it is harder to detect signals if the soil moisture forcing is closer to the range of natural soil moisture variability in the model. Having extremely dry soil moisture forcing allows us to more clearly identify the physical mechanisms. Although we have found clear and consistent responses between the idealized CESM experiments and the extremely dry cases in ERA5 reanalysis data, further studies are warranted to examine if the mechanism found here is sensitive to the strength of SMAs. Second, we only conduct these experiments using one model. While the representation of land-atmosphere interactions may vary among different models, further research is needed to assess the potential model dependency of atmospheric response to dry SMAs. Third, the spatial resolution of the model is relatively coarse (approximately 1°), so neither the topography nor mesoscale processes can be resolved in the current simulations.

Given that the purpose of this study is to bridge the subseasonal to seasonal prediction gap, we are focusing on monthly time scales. The results here should be interpreted as a long-term mean of atmospheric responses to dry soil moisture at a large spatial scale instead of direct impacts of dry SMAs on SALLJ.

5 Conclusions

In this study, three idealized prescribed soil moisture experiments were performed and compared with a control simulation using CESM. The soil moisture within SESA, western SESA, and eastern SESA is prescribed to zero in the experimental simulations to assess the impact of dry SMAs at different locations on the regional climate. Our results show that these experimental runs exhibit distinct precipitation responses associated with anomalous meridional moisture flux. We validated the model simulations by analyzing extremely dry cases over western SESA using ERA5 reanalysis and found similar responses as in the western SESA simulations.

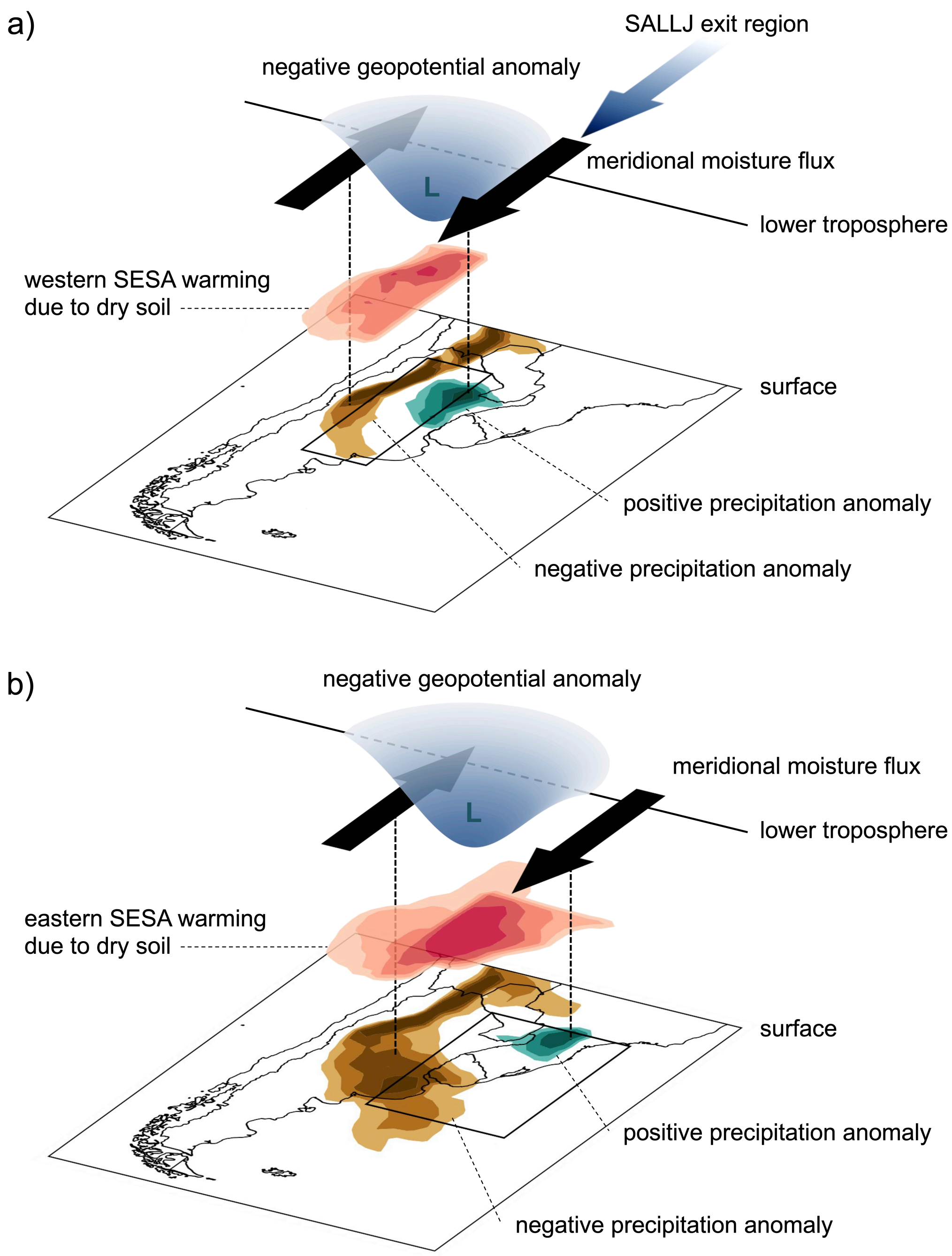

Figure 4. Schematic of the different regional climate responses corresponding to dry soil moisture anomalies over (a) western SESA and (b) eastern SESA. Red shading indicates the anomalous warming at the surface and lower troposphere. Blue shading with the letter L indicates the negative geopotential height anomalies associated with the warming and thermal low at the lower troposphere. Black arrows indicate meridional moisture flux anomalies associated with the geostrophic responses. Green and brown shadings indicate positive and negative precipitation anomalies, respectively. Blue arrow in (a) indicates the SALLJ exit region.

Fig. 4 summarizes the proposed physical mechanism and highlights the distinct climate responses to dry SMAs over western and eastern SESA. On the one hand, when dry SMAs extend over western SESA, the surface warming results in a geostrophic wind anomaly, which is co-located with the SALLJ exit region, enhancing the southward meridional moisture flux and increasing precipitation over northeastern Argentina; near the western boundary of western SESA, the area of anomalous meridional moisture flux is narrower, since it is near the mountain regions and is affected by topography (Fig. 4a). On the other hand, when dry SMAs extend over eastern SESA, the surface warming also leads to changes in geopotential height anomalies, resulting in anomalous southward meridional moisture fluxes on the eastern boundary of the domain and increased precipitation over a small portion of southern Brazil and over the ocean, but the magnitude is smaller because enhanced moisture flux is not co-located with the SALLJ exit region; near the western boundary of the domain, the geopotential height anomalies induce northward meridional fluxes, which are associated with a large area of negative precipitation anomalies (Fig. 4b).

This study provides a causal mechanism of the effect of large-scale SMAs over SESA on precipitation and moisture transport, complementing previous studies. Furthermore, this is the first study to assess the sensitivity of monthly climate response to large-scale SMAs at different locations over SESA. The dry SMAs in western SESA correspond to a negative feedback between soil moisture and precipitation, while the dry SMAs in eastern SESA correspond to a positive feedback. These different relationships between soil moisture and precipitation imply that the location of the dry SMAs may affect the length and intensity of droughts, which have potential implications for subseasonal drought forecasting over SESA.

Open Research

The CESM1 (Hurrell et al., 2013) model code is available at `https://www2.cesm.ucar.edu/models/cesm1.1/`. The ERA5 data (Hersbach et al., 2020) are available at `https://doi.org/10.24381/cds.f17050d7` (variables on single levels) and at `https://doi.org/10.24381/cds.6860a573` (variables on pressure levels). The data and the code used to analyze the results in this study are archived in the University of Illinois' Data Bank (temporary link: `https://databank.illinois.edu/datasets/IDB-0536017?code=P22ca7oGTZNudm-CmKwMhNWGtsTQP17wY5w_X5PUJoQ`, we will replace this temporary link with a permanent DOI upon publication).

Acknowledgments

This work was supported by the National Science Foundation (NSF) award 1852709. We would like to acknowledge high-performance computing support from Cheyenne (doi:10.5065/D6RX99HX) provided by NCAR's Computational and Information Systems Laboratory, sponsored by the NSF. We thank Dr. Haiyan Teng for providing guidance on setting up the CESM experiments and offering valuable advice.

References

Arraut, J. M., Nobre, C., Barbosa, H. M. J., Obregon, G., & Marengo, J. (2012). Aerial rivers and lakes: Looking at large-scale moisture transport and its relation to Amazonia and to subtropical rainfall in South America. *Journal of Climate*, *25*(2), 543–556. doi: 10.1175/2011JCLI4189.1

Baker, J. C. A., Souza, D. C. d., Kubota, P. Y., Buermann, W., Coelho, C. A. S., Andrews, M. B., ... Spracklen, D. V. (2021). An assessment of land–atmosphere interactions over South America using satellites, reanalysis, and two global climate models. *Journal of Hydrometeorology*, *22*(4), 905–922. doi: 10.1175/JHM-D-20-0132.1

Barros, V., Clarke, R., & Silva Días, P. (2006). *Climate change in the La Plata basin.* Retrieved 2023-06-12, from `https://www2.atmos.umd.edu/~berbery/lpb/climate_change_lpb.pdf`

Bieri, C. A., Dominguez, F., & Lawrence, D. M. (2021). Impacts of large-scale soil moisture anomalies on the hydroclimate of southeastern South America. *Journal of Hydrometeorology*, *22*(3), 657–669. doi: 10.1175/JHM-D-20-0116.1

Campbell, M. A., Ferguson, C. R., Burrows, D. A., Beauharnois, M., Xia, G., & Bosart, L. F. (2019). Diurnal effects of regional soil moisture anomalies on the Great Plains low-level jet. *Monthly Weather Review*, *147*(12), 4611–4631. doi: 10.1175/MWR-D-19-0135.1

Chug, D., & Dominguez, F. (2019). Isolating the observed influence of vegetation variability on the climate of La Plata River basin. *Journal of Climate*, *32*(14), 4473–4490. doi: 10.1175/JCLI-D-18-0677.1

Dirmeyer, P. A., Halder, S., & Bombardi, R. (2018). On the harvest of predictability from land states in a global forecast model. *Journal of Geophysical Research: Atmospheres*, *123*(23), 13,111–13,127. doi: 10.1029/2018JD029103

Eltahir, E. A. B. (1998). A soil moisture–rainfall feedback mechanism: 1. Theory and observations. *Water Resources Research*, *34*(4), 765–776. doi: 10.1029/97WR03499

FAO. (2016). *AQUASTAT transboundary river basin overview – La Plata. Food and Agriculture Organization of the United Nations (FAO). Rome, Italy.* Retrieved 2023-06-08, from `https://www.fao.org/publications/card/en/c/CA2141EN/`

Findell, K. L., & Eltahir, E. A. B. (1997). An analysis of the soil moisture-rainfall feedback, based on direct observations from Illinois. *Water Resources Research*, *33*(4), 725–735. doi: 10.1029/96WR03756

Grimm, A. M., Pal, J. S., & Giorgi, F. (2007). Connection between spring conditions and peak summer monsoon rainfall in South America: Role of soil moisture, surface temperature, and topography in eastern Brazil. *Journal of Climate*, *20*(24), 5929–5945. doi: 10.1175/2007JCLI1684.1

Guo, Z., Dirmeyer, P. A., & DelSole, T. (2011). Land surface impacts on subseasonal and seasonal predictability. *Geophysical Research Letters*, *38*(24). doi: 10.1029/2011GL049945

Hersbach, H., Bell, B., Berrisford, P., Hirahara, S., Horányi, A., Muñoz-Sabater, J., … Thépaut, J.-N. (2020). The ERA5 global reanalysis. *Quarterly Journal of the Royal Meteorological Society*, *146*(730), 1999–2049. doi: 10.1002/qj.3803

Hurrell, J. W., Holland, M. M., Gent, P. R., Ghan, S., Kay, J. E., Kushner, P. J., … Marshall, S. (2013). The Community Earth System Model: A framework for collaborative research. *Bulletin of the American Meteorological Society*, *94*(9), 1339–1360. doi: 10.1175/BAMS-D-12-00121.1

Kay, J. E., Deser, C., Phillips, A., Mai, A., Hannay, C., Strand, G., … Vertenstein, M. (2015). The Community Earth System Model (CESM) Large Ensemble project: A community resource for studying climate change in the presence of internal climate variability. *Bulletin of the American Meteorological Society*, *96*(8), 1333–1349. doi: 10.1175/BAMS-D-13-00255.1

Koster, R. D., Chang, Y., & Schubert, S. D. (2014). A mechanism for land–atmosphere feedback involving planetary wave structures. *Journal of Climate*, *27*(24), 9290–9301. doi: 10.1175/JCLI-D-14-00315.1

Koster, R. D., Chang, Y., Wang, H., & Schubert, S. D. (2016). Impacts of local soil moisture anomalies on the atmospheric circulation and on remote surface meteorological fields during boreal summer: A comprehensive analysis over North America. *Journal of Climate*, *29*(20), 7345–7364. doi: 10.1175/JCLI-D-16-0192.1

Koster, R. D., Mahanama, S. P. P., Yamada, T. J., Balsamo, G., Berg, A. A., Boisserie, M., … Wood, E. F. (2011). The second phase of the Global Land–Atmosphere Coupling Experiment: Soil moisture contributions to subseasonal forecast skill. *Journal of Hydrometeorology*, *12*(5), 805–822. doi: 10.1175/2011JHM1365.1

Koster, R. D., & Suarez, M. J. (1995). Relative contributions of land and ocean processes to precipitation variability. *Journal of Geophysical Research: Atmospheres*, *100*(D7), 13775–13790. doi: 10.1029/95JD00176

Marengo, J. A., Soares, W. R., Saulo, C., & Nicolini, M. (2004). Climatology of the low-level jet east of the Andes as derived from the NCEP–NCAR reanalyses: Characteristics and temporal variability. *Journal of Climate*, *17*(12), 2261–2280. doi: 10.1175/1520-0442(2004)017⟨2261:COTLJE⟩2.0.CO;2

Mariotti, A., Ruti, P. M., & Rixen, M. (2018). Progress in subseasonal to seasonal prediction through a joint weather and climate community effort. *npj Climate and Atmospheric Science*, *1*(1), 1–4. doi: 10.1038/s41612-018-0014-z

Matus, S. A., Dominguez, F., & Ford, T. W. (2023). Land and atmosphere conditions prior to extreme Great Plains low-level jets. *Journal of Hydrometeorology*, *24*(4), 783–800. doi: 10.1175/JHM-D-22-0045.1

Monaghan, A. J., Rife, D. L., Pinto, J. O., Davis, C. A., & Hannan, J. R. (2010). Global precipitation extremes associated with diurnally varying low-level jets. *Journal of Climate*, *23*(19), 5065–5084. doi: 10.1175/2010JCLI3515.1

Nicolini, M., Saulo, A. C., Torres, J. C., & Salio, P. (2002). Enhanced precipitation over southeastern South America related to strong low-level jet events during austral warm season. *Meteorologica*, *27*, 59–70.

Oglesby, R. J., & Erickson, D. J. (1989). Soil moisture and the persistence of North American drought. *Journal of Climate*, *2*(11), 1362–1380. doi: 10.1175/1520-0442(1989)002⟨1362:SMATPO⟩2.0.CO;2

Ruscica, R. C., Menéndez, C. G., & Sörensson, A. A. (2016). Land surface–atmosphere interaction in future South American climate using a multi-model ensemble. *Atmospheric Science Letters*, *17*(2), 141–147. doi: 10.1002/asl.635

Ruscica, R. C., Sörensson, A. A., & Menéndez, C. G. (2015). Pathways between soil moisture and precipitation in southeastern South America. *Atmospheric Science Letters*, *16*(3), 267–272. doi: 10.1002/asl2.552

Salio, P., Nicolini, M., & Zipser, E. J. (2007). Mesoscale convective systems over southeastern South America and their relationship with the South American low-level jet. *Monthly Weather Review*, *135*(4), 1290–1309. doi: 10.1175/MWR3305.1

Saulo, C., Ferreira, L., Nogués-Paegle, J., Seluchi, M., & Ruiz, J. (2010). Land–atmosphere interactions during a northwestern Argentina low event. *Monthly Weather Review*, *138*(7), 2481–2498. doi: 10.1175/2010MWR3227.1

Seneviratne, S. I., Corti, T., Davin, E. L., Hirschi, M., Jaeger, E. B., Lehner, I., ... Teuling, A. J. (2010). Investigating soil moisture–climate interactions in a changing climate: A review. *Earth-Science Reviews*, *99*(3), 125–161. doi: 10.1016/j.earscirev.2010.02.004

Shukla, J., & Mintz, Y. (1982). Influence of land-surface evapotranspiration on the Earth's climate. *Science*, *215*(4539), 1498–1501. doi: 10.1126/science.215.4539.1498

Spennemann, P. C., Salvia, M., Ruscica, R. C., Sörensson, A. A., Grings, F., & Karszenbaum, H. (2018). Land-atmosphere interaction patterns in southeastern South America using satellite products and climate models. *International Journal of Applied Earth Observation and Geoinformation*, *64*, 96–103. doi: 10.1016/j.jag.2017.08.016

Spennemann, P. C., & Saulo, A. C. (2015). An estimation of the land-atmosphere coupling strength in South America using the Global Land Data Assimilation System.

International Journal of Climatology, *35*(14), 4151–4166. doi: 10.1002/joc.4274

Sörensson, A. A., & Menéndez, C. G. (2011). Summer soil–precipitation coupling in South America. *Tellus A*, *63*(1), 56–68. doi: 10.1111/j.1600-0870.2010.00468.x

Talib, J., Taylor, C. M., Harris, B. L., & Wainwright, C. M. (2023). Surface-driven amplification of Madden–Julian oscillation circulation anomalies across East Africa and its influence on the Turkana jet. *Quarterly Journal of the Royal Meteorological Society*, *149*(754), 1890–1912. doi: 10.1002/qj.4487

Talib, J., Taylor, C. M., Klein, C., Harris, B. L., Anderson, S. R., & Semeena, V. S. (2022). The sensitivity of the West African monsoon circulation to intraseasonal soil moisture feedbacks. *Quarterly Journal of the Royal Meteorological Society*, *148*(745), 1709–1730. doi: 10.1002/qj.4274

Teng, H., Branstator, G., Tawfik, A. B., & Callaghan, P. (2019). Circumglobal response to prescribed soil moisture over North America. *Journal of Climate*, *32*(14), 4525–4545. doi: 10.1175/JCLI-D-18-0823.1

Vera, C., Baez, J., Douglas, M., Emmanuel, C. B., Marengo, J., Meitin, J., … Zipser, E. (2006). The South American Low-Level Jet Experiment. *Bulletin of the American Meteorological Society*, *87*(1), 63–78. doi: 10.1175/BAMS-87-1-63

Yang, Z., & Dominguez, F. (2019). Investigating land surface effects on the moisture transport over South America with a moisture tagging model. *Journal of Climate*, *32*(19), 6627–6644. doi: 10.1175/JCLI-D-18-0700.1